Title

Tryptophan Can Promote Oxygen Reduction to Water in a Biosynthetic Model of Heme Copper Oxidases

Journal

Biochemistry, 62(2)

ISSN

0006-2960

Authors

Ledray, Aaron P
Dwaraknath, Sudharsan
Chakarawet, Khetpakorn
et al.

Publication Date

2023-01-17

DOI

10.1021/acs.biochem.2c00300

Peer reviewed

Published in final edited form as:

Biochemistry. 2023 January 17; 62(2): 388–395. doi:10.1021/acs.biochem.2c00300.

Tryptophan Can Promote Oxygen Reduction to Water in a Biosynthetic Model of Heme Copper Oxidases

Aaron P. Ledray[†,¶], **Sudharsan Dwaraknath**[‡,¶], **Khetpakorn Chakarawet**[§], **Madeline R. Sponholtz**[‖], **Claire Merchen**[‡], **Casey Van Stappen**[†], **Guodong Rao**[§], **R. David Britt**[§], **Yi Lu**[†,‡,‖,*]

[†]Department of Chemistry, University of Texas at Austin, Austin, TX 78712

[‡]Department of Chemistry, University of Illinois at Urbana-Champaign, Urbana, IL 61801

[§]Department of Chemistry, University of California Davis, CA 95616

[‖]Department of Biochemistry, University of Illinois at Urbana-Champaign, Urbana, IL 61801

Abstract

Heme-copper oxidases (HCOs) utilize tyrosine (Tyr) to donate one of the four electrons required for the reduction of O_2 to water in biological respiration, while tryptophan (Trp) is speculated to fulfill the same role in cyt *bd* oxidases. We previously engineered myoglobin into a biosynthetic model of HCOs and demonstrated the critical role that Tyr serves in the oxygen reduction reaction (ORR). To address the roles of Tyr and Trp in these oxidases, we herein report the preparation of the same biosynthetic model with the Tyr replaced by Trp, and further demonstrate that Trp can also promote the ORR, albeit with lower activity. An X-ray crystal structure of the Trp variant shows a hydrogen bonding network involving two water molecules that are organized by Trp, similar to that in the Tyr variant, which is absent in the crystal structure with the native Phe residue. Additional EPR measurements are consistent with the formation of a Trp radical species upon reacting with H_2O_2. We attribute the lower activity of the Trp variant to Trp's higher reduction potential relative to Tyr. Together, these findings demonstrate - for the first time - that Trp can indeed promote the ORR and provides a structural basis for the observation of varying

[*]Correspondence to: yi.lu@utexas.edu.

[¶]Both authors contributed equally to this work.

Author Contributions:

Y.L. conceived the research and acquired funding. S.D. and A.P.L. performed the experiments with contributions from M.R.S., C.M., C.V.S., K.C., and G.R.. S.D., A.P.L., and K.C. analyzed the data. R.D.B. contributed to EPR data interpretation. Y.L., A.P.L., and S.D. wrote the manuscript. C.V.S revised the manuscript. A.P.L. and S.D. contributed equally to this work.

The authors declare no competing financial interest.

Supporting Information Available:

The Supporting Information is available free of charge at

Rates of water and ROS formation for F33WCuBMb, F33YCuBMb, and CuBMb; optical absorption properties for F33WCuBMb, F33YCuBMb, and CuBMb; X-ray diffraction collection and refinement statistics for the aquoferric F33WCuBMb structure; the Q-band ^{1}H Davies ENDOR spectrum of F33WCuBMb along with simulation parameters; a comparison of X-band EPR spectra between resting state F33YCuBMb, F33WCuBMb, and the reaction of F33WCuBMb with H_2O_2; X-band EPR spectra of wildtype Mb, CuBMb and F33YCuBMb in the absence and presence of H_2O_2; and stopped-flow UV-Vis absorption spectra of F33WCuBMb and F33YCuBMb after reacting with H_2O_2.

Accession Codes:

The protein sequence for sperm whale myoglobin can be accessed as UniProt entry P02185 with the following mutations to create CuBMb: L29H, and F43H. The F33Y and F33W mutations investigated in this work were in addition to the CuBMb mutations.

activities. The results support a redox role for the conserved Trp in *bd* oxidase while suggesting that HCOs use Tyr instead of Trp to achieve higher reactivity.

Graphical Abstract

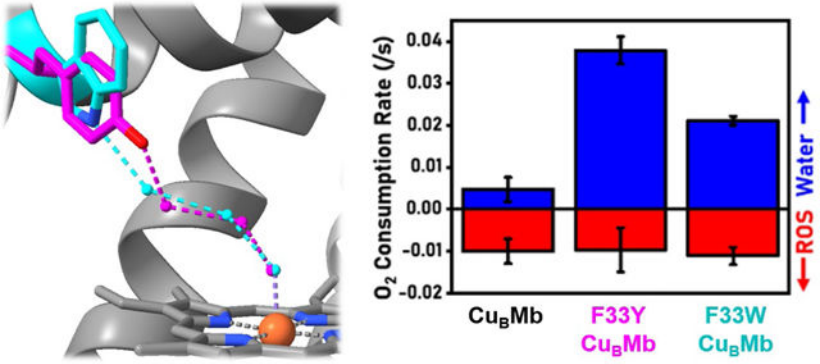

Keywords

Biomimetics; oxygen reduction; artificial metalloenzymes

INTRODUCTION:

Reduction of O_2 to water is fundamental reaction in biological respiration, providing energy for numerous cellular processes.[1] The enzymes responsible for this reaction are terminal oxidases, with heme-copper oxidases (HCOs) as the most well-known example. HCOs contain both heme and a Cu_B center coordinated by three histidine residues, one of which is cross-linked to a neighboring tyrosine (Tyr).

This Tyr is proposed to provide one of the four electrons needed for the $4e^-$ reduction of O_2 to water.[2] However, it has been difficult to elucidate its precise role in the reaction mechanism of native HCOs due to the practical limitations of studying large, membranous enzymes with multiple metal centers. For example, while a Tyr radical species (an intermediate in O_2 reduction) has been observed when HCOs are treated with H_2O_2,[2] such a radical has been difficult to detect when reacting HCOs with O_2.

To address this issue, we and other groups have prepared biomimetic models of HCOs by incorporating Tyr and other phenolic groups in the vicinity of the active site to investigate how an active-site Tyr influences the oxygen reduction reaction (ORR) activity.[3–13] For example, we introduced a Tyr adjacent to the Cu_B site of the biosynthetic HCO model, Cu_BMb, via a Phe33Tyr mutation, mimicking the highly conserved tyrosine residue in HCO (Fig. 1A).[10,14] This variant, F33Y L29H F43H Mb, called F33YCu_BMb, dramatically enhances the rate of the ORR by ~10-fold and increases selectivity for product water from 32% to 80%. These results confirmed the importance of Tyr in the ORR and demonstrated that F33YCu_BMb is a good structural and functional model of HCOs. Using F33YCu_BMb, we were able to detect a tyrosyl radical in its reaction with both H_2O_2 and O_2, providing direct evidence that Tyr can donate an electron in the ORR and that the radical species

previously observed during oxidation of ferric CuBMb with H_2O_2 was consistent with the radical observed upon combining ferrous enzyme with O_2.[12] In further experiments, replacing Tyr33 with non-native tyrosine analogs (OMe-Tyr, Cl-Tyr, F_2-Tyr and F_3-Tyr) showed correlations between the rate of the ORR, the pK_a of the phenolic group[13] and redox potential of Tyr/Tyr·.[15] Since it has been difficult to introduce noncanonical amino acids into native HCOs, our biosynthetic models have allowed us to probe the role of the active-site Tyr in HCOs more precisely than studying native HCOs, even tuning the ORR activity beyond the capabilities of natural amino acids. Beyond its impact on understanding fundamental biology, the ORR is an important reaction of fuel cells that normally requires precious metals, such as platinum, as catalysts. HCOs can catalyze the ORR not only using earth-abundant metal ions (Fe and Cu), but also doing so at a lower overpotential.[16] Therefore, defining the precise role of Tyr and its function in tuning the ORR activity within biosynthetic models contributes to designing novel ORR catalysts through a better understanding of the fundamental principles utilized by Nature.

Despite the well-established role of Tyr in HCOs for ORR, there is one terminal oxidase, *bd* oxidase, which defies the idea that a Tyr is required for ORR. *Bd* oxidase lacks an active-site Tyr, instead sporting a highly conserved (>99%) Trp residue located in the proposed O_2 reduction site.[17] Since both Tyr and Trp residues play redox-active roles in biology,[18–32] the above observation led us to question whether Trp in *bd* oxidase fulfills the same function of Tyr in HCOs. This question is difficult to answer in native HCOs, because Tyr in HCO is cross-linked with one of the copper-coordinating His residues, such that substitution with Trp may perturb the cross-link as well as the properties of the CuB site. Instead, we reasoned that our biosynthetic model would be a facile system in which to answer this question. Towards this goal, we herein report the preparation, spectroscopic and X-ray crystallographic characterization of F33WCuBMb, and compare the effect of an active-site Tyr vs. Trp vs. redox inactive Phe on the oxidase activities of these models.

EXPERIMENTAL SECTION:

All chemicals were purchased from Sigma or Fisher and used without further purification.

Protein expression and purification.

Proteins were expressed and purified following a previously reported protocol,[10] and the identities of the proteins were confirmed by ESI-MS.

Oxidase activity.

Oxygen reduction activity was measured in the Oxygraph Clark type oxygen electrode from Hansatech Instruments Ltd, following a slightly modified form of a reported procedure.[10] The assay was conducted with the internal LED light on and stir speed set to 50. The sample chamber was charged with 850 μL of 100 mM KPi pH 6.0 buffer and then 50 μL of a solution containing 40 mM N,N,N’,N’-tetramethyl-p-phenylenediamine dihydrochloride, a redox mediator, and 400 mM sodium ascorbate, the terminal reductant, was added. The O_2 concentration was monitored, and data collected until at least 30 seconds of a linear trace of [O_2] vs. time was observed, which would be used to do background subtraction during

data processing. Then, 100 μL of a 200 μM stock of protein was added rapidly, resulting in an assay enzyme concentration of 20 μM. Data was collected for at least 60 s thereafter. The measurement of the rate of O_2 consumption was done using the rate measurement tool within the Oxygraph software itself. Specifically, a line was drawn to fit the data, starting from 30s after protein injection and ending at 60 s after protein injection. The ORR activity of each Mb variant was measured in triplicate.

The rates of water and ROS formation were determined by measuring O_2 consumption rates in the absence and presence of the ROS scavenger, catalase, and then plugging these values into equations reported earlier.[10]

Protein crystallography.

A crystal of aquoferric F33W Cu_BMb was grown by hanging drop vapor diffusion in a 24-well tray purchased from Hampton Research Inc. Crystallization solution was composed of 0.1M MES pH 6.1, 0.2M NaOAc x $3H_2O$ and 25% PEG 6000. Protein was concentrated to ~1 mM in 100 mM potassium phosphate pH 7 buffer. Solutions were mixed 1:1 to yield a final drop volume of 4 μL, which was equilibrated against 300 μL of well buffer at 4^o C. Crystals appeared within 1 week. At the time of observation of crystals, the well was not sealed completely by the coverslip, likely allowing for faster evaporation than usual for a properly sealed well.

Diffraction data were collected at the Advanced Light Source beamline 5.0.2. Data reduction and scaling were performed in MOSFLM[33] and Aimless, respectively. The structure was solved by isomorphous replacement with the polypeptide and heme cofactor of PDB: 4FWX.[10] Phasing and refinement were performed in Phenix[34] and model building in Coot.[35] Graphics were generated using PyMol.

Optical Absorption Properties.

UV-Vis spectra shown here and in the main text were collected on a Varian Cary 5000 spectrophotometer. Extinction coefficients were obtained using an Agilent 8453 spectrophotometer. Aquoferric heme Soret extinction coefficients were determined by a hemochromagen assay described earlier.[36] The extinction coefficient of deoxyferrous heme Soret bands were obtained by first treating a solution of the aquoferric protein with dithionite in an anaerobic chamber. Then, the ratio of the Soret band absorbances of deoxyferrous and aquoferric species was calculated (values range from 0.7 – 0.9), and this value was multiplied by the extinction coefficient of the corresponding aquoferric heme Soret, yielding the extinction coefficient of the deoxyferrous heme Soret.

Electron paramagnetic resonance spectroscopy.

The F33WCu_BMb + 1 equiv H_2O_2 sample was prepared by mixing a solution of 10 mM protein containing 20% glycerol with equal volume of 10 mM H_2O_2, then injecting this mixture at 5 seconds directly into liquid nitrogen to yield a final protein concentration of 5 mM. The frozen reaction solution was then crushed into a powder and loaded into an EPR tube (2.00 mm ID, 2.40 mm OD).

EPR spectra were recorded at the CalEPR center in the Department of Chemistry, University of California, Davis. Continuous wave (CW) X-Band (9.39 GHz) spectra were collected using a Bruker Biospin EleXsys E500 spectrometer (Billerica, MA) equipped with a super high Q resonator (ER4122SHQE). Cryogenic temperatures were controlled and maintained through the use of an ESR900 liquid helium cryostat in conjunction with a temperature controller (Oxford Instruments ITC503) and a gas flow controller.

Echo-detected field sweep spectra at Q-band (34 GHz) were collected using a Bruker Biospin EleXsys E580 spectrometer equipped with a 10 W amplifier and an R. A. Isaacson-built cylindrical TE011 resonator mounted in an Oxford CF935 cryostat. The standard Hahn echo sequence (: $\pi/2 - \tau - \pi -$ echo) was applied to the sample via the XEPR software at various magnetic field values. ENDOR measurements were performed at 50 K by employing the Davies pulse sequence: $\pi -$ RF $- \pi/2 - \tau - \pi - \tau$-echo ($\pi/2 = 12$ ns, RF pulse = 20 μs, $\tau = 300$ ns).

RESULTS AND DISCUSSION:

To determine whether Trp can support ORR activity, we measured the ORR activity of F33WCuBMb in comparison with those of CuBMb and F33YCuBMb variants under the same conditions. F33WCuBMb reduces O_2 to water at 4x the rate of CuBMb, while generating the same amount of reactive oxygen species (ROS) (Fig. 2, Table S1). This selective enhancement in the rate of water formation, without change in ROS formation, suggests that an active-site Trp may indeed replace Tyr and participate in the 4 e^- reduction of O_2 to water, which is unprecedented in biomimetic studies of biological respiration.

To understand why F33WCuBMb and F33YCuBMb display similar ORR activity, we obtained a 1.3 Å crystal structure of ferric F33WCuBMb (Fig. 1B, PDB: 8EKO) and compared it to the structure of ferric F33YCuBMb (Fig. 1A, PDB: 4FWX).[10] First, both the overall protein and active site structures of the two variants appear very similar (Fig. 1C, RMSD 0.329 Å), including the conformation of the heme cofactors and the orientation of the Trp33/Tyr33 sidechains. For example, the distance from C_β carbons of Trp33 and Tyr33 to the nearest heme edge sp^2 carbon are 10.3 and 9.9 Å, respectively. These observations are corroborated by the UV-Vis absorption spectra in solution, which reveal that both the ferric (Fig. 3) and deoxyferrous (Fig. S1) forms of F33WCuBMb exhibit spectra that are nearly identical to those of F33YCuBMb with regards to the energetic positions of the heme Soret and Q bands, indicating similar geometric structures (Table S2). However, the relative intensities of these bands, particularly between the Q bands, vary significantly. Previous studies have attributed such differences in intensities to the polarity of the environment surrounding the heme site,[37] presently rendered by Phe, Tyr and Trp. Since polarity may influence the strength of the hydrogen bonding network around the heme center and the hydrogen bonding network plays an important role in ORR, this difference in Q band intensity may help explain their difference in activity.

Importantly, it has previously been shown that Tyr33 organizes a hydrogen bonding network involving ordered water molecules in the active-site (Fig. 1a)[10] that plays a key role in facilitating proton coupled electron transfer from Tyr33 to the heme-bound oxygen. The

crystal structure of F33WCuBMb obtained in this work reveals that the indole N of Trp33 is also capable of organizing a similar hydrogen bonding network involving two water molecules (Fig. 1b). Therefore, we attribute this hydrogen bonding network as the major contributor enabling ORR activity in F33WCuBMb, and similarly in F33YCuBMb. This hydrogen bonding network is also consistent with the crystal structure of F33YCuBMb with oxygen bound (PDB: 5HAV), suggesting that the water network we report in the ferric crystal structure (Fig. 1b) is relevant to the O_2-substrate bound F33WCuBMb.

Although F33WCuBMb exhibits ORR activity and produces a comparable quantity of ROS, the rate of water formation is about half that of F33YCuBMb. As a minimal number of structural differences are observed between the two variants, we attribute variations in the ORR activity of the two variants to the difference in proton-coupled reduction potentials (E°′) between Tyr and Trp. It is known that free Trp normally exhibits a higher E°′ than Tyr in solution.[38] While it is usually extremely difficult to measure E°′ for Trp and Tyr in a protein matrix due to the presence of Trp and Tyr in other locations of the same protein (as well as other redox cofactors such as heme), measurements of E°′ for these residues have been reported in a very simple α_3X model protein in which there is no such interference.[39] The E°′ of Trp was found to be 109 mV higher than that of Tyr across the biological pH range. While Trp and Tyr can both span a wide range of protein reduction potentials in different proteins (due to the effects of different residues surrounding Trp or Tyr), we anticipate that this trend - E°′(Trp) > E°′(Tyr) – will hold true when in an otherwise identical environment. Based on this reasoning, Trp33 in F33WCuBMb is expected to follow a similar trend as in the above α_3X model protein and thus exhibit a higher E°′ than Tyr33 in F33YCuBMb. Similarly, the pK_a of Trp33 is expected to be higher than Tyr33, which would contribute to a slower reaction in a proton-dependent process. The free amino acid Trp has a side-chain pK_a of 16.8, compared to the side-chain pK_a of 10.6 for the amino acid Tyr.[40,41] In a protein, Tyr's side-chain pK_a has been reported at 10.2.[42] We believe that in the same structural environment such as that between F33WCuBMb and F33YCuBMb, the difference in pK_a between free amino acids Tyr/Trp will remain.

Consistent with our previous study on F33YCuBMb,[12] we have found that reaction of the oxidized F33WCuBMb with a single equivalent of H_2O_2 generates a protein radical species. Similar to F33YCuBMb, the resting state F33WCuBMb displays an EPR signal typical of water-bound high-spin ferric myoglobin (Fig. S2).[43] The radical signal observed in F33WCuBMb upon reaction with H_2O_2 is notably different than the spectrum observed in CuBMb without the Phe33 mutations, while also displaying features unique from the F33YCuBMb Tyr radical (Fig. 4). After reacting with H_2O_2, a relatively stable Compound II species (Fe(IV)=O, $S = 1$ EPR-silent) is generated, having first made a short-lived Compound I intermediate (Fe(IV)=O + porphyrin radical, or formally an Fe(V) species)[44] which is then reduced by a single electron.

The continuous wave (CW) X-band (9.391 GHz) EPR spectrum of the radical intermediate trapped after 5 s reaction time displays a prominent doublet feature, indicating a strong hyperfine coupling to magnetic nuclei (Figure 4, top). Tryptophan radical is known to exhibit complicated and drastically different EPR features depending on the environment in which it is located[45] due to extensive hyperfine interactions with N, β-H, as well as

aromatic H nuclei.[46,47] In our X-band spectrum, the lack of fine structure precludes a detailed analysis of the generated radical, although the doublet feature is reminiscent of a tryptophan radical generated by H_2O_2 reaction with the versatile peroxidase in *P. eryngii*.[45] To further confirm the identity of the generated radical, the same EPR sample was measured at Q-band frequency (34.297 GHz). The Q-band echo-detected field-sweep spectrum of trapped intermediate in F33WCuBMb oxidation showcases a broad peak centered around $g = 2.00355$ (Figure 4, bottom). The g-tensor obtained from the Q-band spectrum is noticeably larger than that of a typical carbon-based radical, suggesting the existence of a N-based radical. This value is in good agreement with the values previously reported for a tryptophan radical; for example, Trp radicals in azurin ($g = [2.004, 2.003, 2.002]$),[46,47] versatile peroxidase (isotropic $g \sim 2.0027$),[45] and ribonucleotide reductase (Y122F mutant, $g = [2.0033, 2.0024, 2.0021]$).[48,49] We note that tyrosyl radicals exhibit larger g anisotropy due to the heavier O atom, such as in F33YCuBMb ($g = [2.0076, 2.0044, 2.0021]$)[12] and wildtype ribonucleotide reductase ($g = [2.0091, 2.0046, 2.0021]$).[49] We therefore attribute the EPR signals observed in F33WCuBMb to a Trp radical on the Trp33 residue (Fig. 4).

Further Q-band ^{1}H ENDOR measurements were performed to resolve the hyperfine interactions of the Trp radical (see SI). The resulting spectrum features several sharp peaks with hyperfine couplings below 5 MHz and a broad feature spanning ca. 25 MHz (Fig. 4, bottom). The broad feature was reasonably simulated by a hyperfine coupling tensor $A(^1H) = [12, 12, 25]$ MHz, approximately. This value is in reasonable agreement with hyperfine coupling to the β-H of Trp reported elsewhere.[45–47] Using this A-tensor, reasonable simulations of the X- and Q-band data can be obtained (Figure 4, red lines). The resulting spectra were simulated using $g_{iso} = 2.00355$, $A(^{14}N) = [14, 14, 33]$ MHz, and three ^{1}H hyperfine coupling tensors derived from the ^{1}H ENDOR spectrum (Table S4). We note that the g anisotropy of the presumed tryptophan radical cannot be fully resolved at Q-band frequency, and thus we have treated the simulation with an isotropic model. Discrepancies between the data and simulations at X-band may be attributed to this simplification of the hyperfine coupling scheme.

Since F33WCuBMb can perform the ORR (which needs both electrons and protons), we believe Trp33 is able to perform both proton transfer and electron transfer rather than electron transfer alone, coupling a proton transfer step to a solvent water molecule to an electron transfer to the ferryl moiety. This step appears to occur concurrently with generation of Compound II – this is because the reaction of CuBMb with H_2O_2 produces (similar to wildtype myoglobin) a smooth transition from resting state ferric to Compound II, bypassing accumulation of Compound I (Fe(IV) porphyrin cationic radical, formally Fe(V)) and instead showing the Fe(IV)=O state (Fig. S6).

Previous work from our group suggests a proton-coupled process for the generation of the Tyr• in F33YCuBMb, as replacing the Tyr33 position with noncanonical amino acid tyrosine analogues containing halogen substituents (thus spanning a pK_a range of 6.4 – 10).[13] It was observed that the ORR activity in terms of O_2 consumption and H_2O product formation over ROS increased linearly as the Tyr33-analogue's pK_a was lowered. Similarly, we see the same effect between Tyr33/Trp33, as the pK_a of residue 33 in CuBMb should be elevated (all else being equal) and correspondingly H_2O product yield decreases (Fig 3). Specifically, we

have shown that by replacing Tyr with Trp, a similar radical is produced upon reaction with H_2O_2, with a decreased rate of water formation under steady-state conditions that aligns with our understanding of Trp's elevated pK_a and E°´.

CONCLUSION:

In conclusion, we have shown for the first time that the Tyr in the active site of a functional HCO model in myoglobin can be replaced with Trp while maintaining functional ORR activity. We attribute the reduced rate of water formation in the Trp-containing mutant to the higher E°´ of Trp33 relative to Tyr33, resulting in a lower driving force for electron transfer from Trp33 to the heme-bound oxygen species. While Trp and Tyr seemingly can perform the same $1e^-$ redox function, they are highly conserved when playing a role in enzymatic redox functions. There are only a few reported exceptions where the residues have been interchanged in nature.[50–52] However, this kind of mutation is very difficult to carry out in native HCOs, where Tyr forms a crosslink with a nearby His. Perturbation of this crosslink could very well abolish activity altogether, hindering fine analysis of the role of the chemical properties of Tyr versus Trp in oxidase activity. Our findings support a redox role for the conserved Trp in cyt *bd* oxidases while suggesting that HCOs uses Tyr instead of Trp due to the higher reactivity observed with Tyr, although Trp can support O_2 reduction.

It has long been proposed that biology uses the protein milieu to tune the properties of Tyr and Trp for their appropriate functions.[53–58] However, very little is known about how this is accomplished due to the difficulty in isolating redox events of specific Tyr and Trp residues from other amino acids and cofactors in proteins. This work demonstrates the unique strength of biosynthetic modeling in teasing out subtle, but critical, structure-function relationships in complex heteronuclear metalloenzymes driving biological energy transduction. While we can only speculate about the evolutionary role a conserved Trp residue serves in cyt *bd* oxidases, we argue that the activities of cyt *bd* oxidases have been refined by residues in the active site to favor O_2 reduction at a particular rate - and not necessarily the fastest – through a Trp residue that still supports proton-coupled electron transfer and the same functional role of a Tyr. Our model suggests that Trp can serve as an intermediary electron source through a proton-coupled electron transfer step in our functional model of HCO.

Supplementary Material

Refer to Web version on PubMed Central for supplementary material.

ACKNOWLEDGMENT:

We thank Dr. Matthew W. Waugh for helpful discussions about enzyme kinetics, and both Rachel Martini and Dr. Evan Mirts for technical assistance.

Funding Sources:

This material is based upon work supported by the National Institute of General Medical Sciences of the National Institutes of Health under award number GM141931 (to YL) and by the National Science Foundation Graduate Research Fellowship to SD under Grant No. DGE – 1746047. We also thank the Robert A. Welch Foundation (Grant F-0020) for support of the Lu group research program at the University of Texas at Austin.

Beamline 5.0.2 of the Advanced Light Source, a U.S. DOE Office of Science User Facility under Contract No. DE-AC02-05CH11231, is supported in part by the ALS-ENABLE program funded by the National Institutes of Health, National Institute of General Medical Sciences, grant P30 GM124169-01. EPR spectroscopic studies were funded by the National Institutes of Health (NIH 1R35GM126961 to R.D.B.).

REFERENCES:

(1). Babcock GT (1999) How oxygen is activated and reduced in respiration. Proc. Natl. Acad. Sci. U. S. A 96, 12971–12973.

(2). Yu MA, Egawa T, Shinzawa-Itoh K, Yoshikawa S, Guallar V, Yeh S-R, Rousseau DL, and Gerfen GJ (2012) Two tyrosyl radicals stabilize high oxidation states in cytochrome C oxidase for efficient energy conservation and proton translocation. J. Am. Chem. Soc 134, 4753–61. [PubMed: 22296274]

(3). Liu J-G, Naruta Y, Tani F, Chishiro T, and Tachi Y. (2004) Formation and spectroscopic characterization of the dioxygen adduct of a heme –Cu complex possessing a cross-linked tyrosine– histidine mimic: modeling the active site of cytochrome c oxidase. Chem. Commun 0, 120–121.

(4). Kim E, Kamaraj K, Galliker B, Rubie ND, Moënne-Loccoz P, Kaderli S, Zuberbühler AD, and Karlin KD (2005) Dioxygen Reactivity of Copper and Heme−Copper Complexes Possessing an Imidazole−Phenol Cross-Link. Inorg. Chem 44, 1238–1247. [PubMed: 15732964]

(5). Collman JP, Decréau RA, and Sunderland CJ (2006) Single-turnover intermolecular reaction between a FeIII–superoxide–CuI cytochrome c oxidase model and exogeneous Tyr244 mimics. Chem. Commun 3894–3896.

(6). Collman JP, Devaraj NK, Decréau RA, Yang Y, Yan Y-L, Ebina W, Eberspacher TA, and Chidsey CED (2007) A Cytochrome c Oxidase Model Catalyzes Oxygen to Water Reduction Under Rate-Limiting Electron Flux. Science 315, 1565–1568. [PubMed: 17363671]

(7). Charalambidis G, Ladomenou K, Boitrel B, and Coutsolelos AG (2009) Synthesis and Studies of a Super-Structured Porphyrin Derivative – A Potential Building Block for CcO Mimic Models. E. J. Org. Chem 2009, 1263–1268.

(8). Ladomenou K, Charalambidis G, and Coutsolelos AG (2010) Spectroscopic and electrochemical studies of novel model compounds for cytochrome c oxidase. Inorg. Chim. Acta 363, 2201–2208.

(9). Liu X, Yu Y, Hu C, Zhang W, Lu Y, and Wang J. (2012) Significant Increase of Oxidase Activity through the Genetic Incorporation of a Tyrosine–Histidine Cross-Link in a Myoglobin Model of Heme–Copper Oxidase. Angew. Chem., Int. Ed 51, 4312–4316.

(10). Miner KD, Mukherjee A, Gao Y-G, Null EL, Petrik ID, Zhao X, Yeung N, Robinson H, and Lu Y. (2012) A Designed Functional Metalloenzyme that Reduces O2 to H2O with Over One Thousand Turnovers. Angew. Chem., Int. Ed 51, 5589–5592.

(11). Ladomenou K, Charalambidis G, and Coutsolelos AG (2013) CO and O2 binding studies of new model complexes for CcO. Polyhedron 54, 47–53.

(12). Yu Y, Mukherjee A, Nilges MJ, Hosseinzadeh P, Miner KD, and Lu Y. (2014) Direct EPR Observation of a Tyrosyl Radical in a Functional Oxidase Model in Myoglobin during both H_2O_2 and O_2 Reactions. J. Am. Chem. Soc 136, 1174–1177. [PubMed: 24383850]

(13). Yu Y, Lv X, Li J, Zhou Q, Cui C, Hosseinzadeh P, Mukherjee A, Nilges MJ, Wang J, and Lu Y. (2015) Defining the Role of Tyrosine and Rational Tuning of Oxidase Activity by Genetic Incorporation of Unnatural Tyrosine Analogs. J. Am. Chem. Soc 137, 4594–4597. [PubMed: 25672571]

(14). Petrik ID, Davydov R, Ross M, Zhao X, Hoffman B, and Lu Y. (2016) Spectroscopic and Crystallographic Evidence for the Role of a Water-Containing H-Bond Network in Oxidase Activity of an Engineered Myoglobin. J. Am. Chem. Soc 138, 1134–1137. [PubMed: 26716352]

(15). Yu Y, Zhou Q, Wang L, Liu X, Zhang W, Hu M, Dong J, Li J, Lv X, Ouyang H, Li H, Gao F, Gong W, Lu Y, and Wang J. (2015) Significant improvement of oxidase activity through the genetic incorporation of a redox-active unnatural amino acid. Chem. Sci 6, 3881–3885. [PubMed: 26417427]

(16). Kjaergaard CH, Rossmeisl J, and Nørskov JK (2010) Enzymatic versus Inorganic Oxygen Reduction Catalysts: Comparison of the Energy Levels in a Free-Energy Scheme. Inorg. Chem 49, 3567–3572. [PubMed: 20380458]

(17). Safarian S, Rajendran C, Müller H, Preu J, Langer JD, Ovchinnikov S, Hirose T, Kusumoto T, Sakamoto J, and Michel H. (2016) Structure of a bd oxidase indicates similar mechanisms for membrane-integrated oxygen reductases. Science 352, 583–586. [PubMed: 27126043]

(18). Li YF, Heelis PF, and Sancar A. (1991) Active site of DNA photolyase: tryptophan-306 is the intrinsic hydrogen atom donor essential for flavin radical photoreduction and DNA repair in vitro. Biochemistry 30, 6322–9. [PubMed: 2059637]

(19). Stubbe J, and van der Donk WA (1998) Protein Radicals in Enzyme Catalysis. Chem. Rev 98, 705–762. [PubMed: 11848913]

(20). Aubert C, Mathis P, Eker APM, and Brettel K. (1999) Intraprotein electron transfer between tyrosine and tryptophan in DNA photolyase from Anacystis nidulans. Proc. Natl. Acad. Sci. U. S. A 96, 5423–5427. [PubMed: 10318899]

(21). Aubert C, Vos MH, Mathis P, Eker AP, and Brettel K. (2000) Intraprotein radical transfer during photoactivation of DNA photolyase. Nature 405, 586–90. [PubMed: 10850720]

(22). Pogni R, Baratto MC, Giansanti S, Teutloff C, Verdin J, Valderrama B, Lendzian F, Lubitz W, Vazquez-Duhalt R, and Basosi R. (2005) Tryptophan-Based Radical in the Catalytic Mechanism of Versatile Peroxidase from *Bjerkandera adusta*. Biochemistry 44, 4267–4274. [PubMed: 15766255]

(23). Gray HB, and Winkler JR (2010) Electron flow through metalloproteins. Biochim. Biophys. Acta, Bioenerg 1797, 1563–1572.

(24). Miner KD, Pfister TD, Hosseinzadeh P, Karaduman N, Donald LJ, Loewen PC, Lu Y, and Ivancich A. (2014) Identifying the Elusive Sites of Tyrosyl Radicals in Cytochrome c Peroxidase: Implications for Oxidation of Substrates Bound at a Site Remote from the Heme. Biochemistry 53, 3781–3789. [PubMed: 24901481]

(25). Gray HB, and Winkler JR (2015) Hole hopping through tyrosine/tryptophan chains protects proteins from oxidative damage. Proc. Natl. Acad. Sci. U. S. A 112, 10920–10925.

(26). Oldemeyer S, Franz S, Wenzel S, Essen L-O, Mittag M, and Kottke T. (2016) Essential Role of an Unusually Long-lived Tyrosyl Radical in the Response to Red Light of the Animal-like Cryptochrome aCRY. J. Biol. Chem 291, 14062–14071.

(27). Lin C, Top D, Manahan CC, Young MW, and Crane BR (2018) Circadian clock activity of cryptochrome relies on tryptophan-mediated photoreduction. Proc. Natl. Acad. Sci. U. S. A 115, 3822–3827. [PubMed: 29581265]

(28). Geng J, Dornevil K, Davidson VL, and Liu A. (2013) Tryptophan-mediated charge-resonance stabilization in the bis-Fe(IV) redox state of MauG. Proc. Natl. Acad. Sci. U. S. A 110, 9639–44. [PubMed: 23720312]

(29). Shin I, Ambler BR, Wherritt D, Griffith WP, Maldonado AC, Altman RA, and Liu A. (2018) Stepwise O-Atom Transfer in Heme-Based Tryptophan Dioxygenase: Role of Substrate Ammonium in Epoxide Ring Opening. J. Am. Chem. Soc 140, 4372–4379. [PubMed: 29506384]

(30). Geng J, Weitz AC, Dornevil K, Hendrich MP, and Liu A. (2020) Kinetic and Spectroscopic Characterization of the Catalytic Ternary Complex of Tryptophan 2,3-Dioxygenase. Biochemistry 59, 2813–2822. [PubMed: 32659080]

(31). Abu Tarboush N, Jensen LMR, Feng M, Tachikawa H, Wilmot CM, and Davidson VL (2010) Functional Importance of Tyrosine 294 and the Catalytic Selectivity for the Bis-Fe(IV) State of MauG Revealed by Replacement of This Axial Heme Ligand with Histidine. Biochemistry 49, 9783–9791. [PubMed: 20929212]

(32). Tarboush NA, Jensen LMR, Yukl ET, Geng J, Liu A, Wilmot CM, and Davidson VL (2011) Mutagenesis of tryptophan199 suggests that hopping is required for MauG-dependent tryptophan tryptophylquinone biosynthesis. Proc. Natl. Acad. Sci. U. S. A 108, 16956–16961.

(33). Battye TGG, Kontogiannis L, Johnson O, Powell HR, and Leslie AGW (2011) iMOSFLM: a new graphical interface for diffraction-image processing with MOSFLM. Acta Crystallogr., Sect. D: Biol. Crystallogr 67, 271–281. [PubMed: 21460445]

(34). Liebschner D, Afonine PV, Baker ML, Bunkóczi G, Chen VB, Croll TI, Hintze B, Hung L-W, Jain S, McCoy AJ, Moriarty NW, Oeffner RD, Poon BK, Prisant MG, Read RJ, Richardson JS, Richardson DC, Sammito MD, Sobolev OV, Stockwell DH, Terwilliger TC, Urzhumtsev AG, Videau LL, Williams CJ, and Adams PD (2019) Macromolecular structure determination using X-rays, neutrons and electrons: recent developments in Phenix. Acta Crystallogr., Sect. D: Biol. Crystallogr 75, 861–877.

(35). Emsley P, Lohkamp B, Scott WG, and Cowtan K. (2010) Features and development of *Coot*. Acta Crystallogr D Biol Crystallogr 66, 486–501. [PubMed: 20383002]

(36). Barr I, and Guo F. (2015) Pyridine Hemochromagen Assay for Determining the Concentration of Heme in Purified Protein Solutions. Bio Protoc 5.

(37). Cowan JA, and Gray HB (1989) Q-band splitting in the spectra of heme proteins. Inorg. Chem 28, 4554–4556.

(38). Mahmoudi L, Kissner R, Nauser T, and Koppenol WH (2016) Electrode Potentials of l-Tryptophan, l-Tyrosine, 3-Nitro-l-tyrosine, 2,3-Difluoro-l-tyrosine, and 2,3,5-Trifluoro-l-tyrosine. Biochemistry 55, 2849–2856. [PubMed: 27144928]

(39). Glover SD, Tyburski R, Liang L, Tommos C, and Hammarström L. (2018) Pourbaix Diagram, Proton-Coupled Electron Transfer, and Decay Kinetics of a Protein Tryptophan Radical: Comparing the Redox Properties of W32• and Y32• Generated Inside the Structurally Characterized α3W and α3Y Proteins. J. Am. Chem. Soc 140, 185–192. [PubMed: 29190082]

(40). Yagil G. (1967) The proton dissociation constant of pyrrole, indole and related compounds. Tetrahedron 23, 2855–2861. [PubMed: 6047529]

(41). Henchoz Y, Schappler J, Geiser L, Prat J, Carrupt P-A, and Veuthey J-L (2007) Rapid determination of pKa values of 20 amino acids by CZE with UV and capacitively coupled contactless conductivity detections. Anal Bioanal Chem 389, 1869–1878. [PubMed: 17874082]

(42). Oktaviani NA, Pool TJ, Kamikubo H, Slager J, Scheek RM, Kataoka M, and Mulder FAA (2012) Comprehensive Determination of Protein Tyrosine pKa Values for Photoactive Yellow Protein Using Indirect 13C NMR Spectroscopy. Biophys. J 102, 579–586. [PubMed: 22325281]

(43). Egeberg KD, Springer BA, Martinis SA, Sligar SG, Morikis D, and Champion PM (1990) Alteration of sperm whale myoglobin heme axial ligation by site-directed mutagenesis. Biochemistry 29, 9783–9791. [PubMed: 2176857]

(44). Egawa T, Shimada H, and Ishimura Y. (2000) Formation of Compound I in the Reaction of Native Myoglobins with Hydrogen Peroxide. J. Biol. Chem 275, 34858–34866.

(45). Pogni R, Teutloff C, Lendzian F, and Basosi R. (2007) Tryptophan radicals as reaction intermediates in versatile peroxidases: Multifrequency EPR, ENDOR and density functional theory studies. Appl. Magn. Reson 31, 509–526.

(46). Shafaat HS, Leigh BS, Tauber MJ, and Kim JE (2010) Spectroscopic Comparison of Photogenerated Tryptophan Radicals in Azurin: Effects of Local Environment and Structure. J. Am. Chem. Soc 132, 9030–9039. [PubMed: 20536238]

(47). Stoll S, Shafaat HS, Krzystek J, Ozarowski A, Tauber MJ, Kim JE, and Britt RD (2011) Hydrogen Bonding of Tryptophan Radicals Revealed by EPR at 700 GHz. J. Am. Chem. Soc 133, 18098–18101.

(48). Lendzian F, Sahlin M, MacMillan F, Bittl R, Fiege R, Pötsch S, Sjöberg B-M, Gräslund A, Lubitz W, and Lassmann G. (1996) Electronic Structure of Neutral Tryptophan Radicals in Ribonucleotide Reductase Studied by EPR and ENDOR Spectroscopy. J. Am. Chem. Soc 118, 8111–8120.

(49). Bleifuss G, Kolberg M, Pötsch S, Hofbauer W, Bittl R, Lubitz W, Gräslund A, Lassmann G, and Lendzian F. (2001) Tryptophan and Tyrosine Radicals in Ribonucleotide Reductase: A Comparative High-Field EPR Study at 94 GHz. Biochemistry 40, 15362–15368.

(50). Biskup T, Paulus B, Okafuji A, Hitomi K, Getzoff ED, Weber S, and Schleicher E. (2013) Variable Electron Transfer Pathways in an Amphibian Cryptochrome: Tryptophan versus tyrosine-based radical pairs. J. Biol. Chem 288, 9249–9260. [PubMed: 23430261]

(51). Nohr D, Franz S, Rodriguez R, Paulus B, Essen L-O, Weber S, and Schleicher E. (2016) Extended Electron-Transfer in Animal Cryptochromes Mediated by a Tetrad of Aromatic Amino Acids. Biophys. J 111, 301–311. [PubMed: 27463133]

(52). Holub D, Ma H, Krauß N, Lamparter T, Elstner M, and Gillet N. (2018) Functional role of an unusual tyrosine residue in the electron transfer chain of a prokaryotic (6–4) photolyase. Chem. Sci 9, 1259–1272. [PubMed: 29675172]

(53). Tommos C, Skalicky JJ, Pilloud DL, Wand AJ, and Dutton PL (1999) De Novo Proteins as Models of Radical Enzymes. Biochemistry 38, 9495–9507. [PubMed: 10413527]

(54). Westerlund K, Moran SD, Privett HK, Hay S, Jarvet J, Gibney BR, and Tommos C. (2008) Making a single-chain four-helix bundle for redox chemistry studies. Protein Eng., Des. Sel 21, 645–652. [PubMed: 18755707]

(55). Smith AT, Doyle WA, Dorlet P, and Ivancich A. (2009) Spectroscopic evidence for an engineered, catalytically active Trp radical that creates the unique reactivity of lignin peroxidase. Proc. Natl. Acad. Sci. U. S. A 106, 16084–16089.

(56). Warren JJ, Winkler JR, and Gray HB (2012) Redox Properties of Tyrosine and Related Molecules. FEBS Lett 586, 596–602. [PubMed: 22210190]

(57). Glover SD, Jorge C, Liang L, Valentine KG, Hammarström L, and Tommos C. (2014) Photochemical Tyrosine Oxidation in the Structurally Well-Defined α3Y Protein: Proton-Coupled Electron Transfer and a Long-Lived Tyrosine Radical. J. Am. Chem. Soc 136, 14039–14051.

(58). Payne TM, Yee EF, Dzikovski B, and Crane BR (2016) Constraints on the radical cation center of cytochrome c peroxidase for electron transfer from cytochrome c. Biochemistry 55, 4807–4822. [PubMed: 27499202]

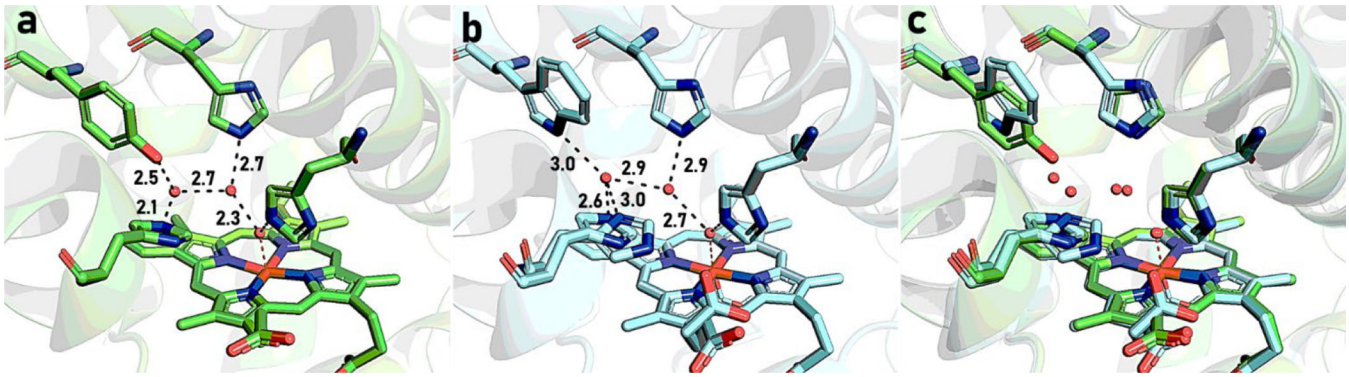

Figure 1.

Crystal structures of aquoferric forms of a) F33YCuBMb (PDB: 4FWX), b) F33WCuBMb (PDB: 8EKO), and c) the overlay of the two structures. There is no copper ion in these structures, despite the enzyme name CuBMb – the laboratory has historically investigated the CuBMb-series of mutant enzymes with and without copper and uses the terminology Cu(I)-CuBMb to reflect Cu(I)-bound CuBMb, and CuBMb to refer to copper-free enzyme.

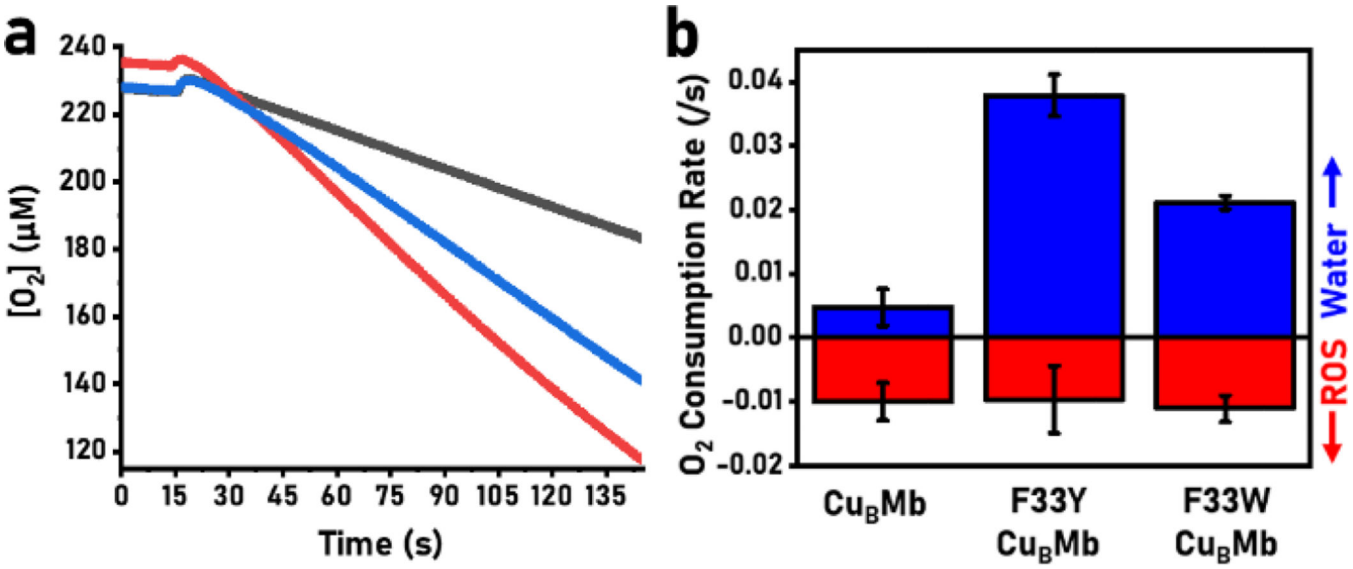

Figure 2.

(a) Measured O_2 consumption traces of 20 μM CuBMb (gray), F33YCuBMb (red), and F33WCuBMb (blue) in 100 mM KPi pH 6 buffer containing 100 eq. of TMPD and 1000 eq. of ascorbate. (b) Calculated rates of water and ROS formation for the three enzyme variants.

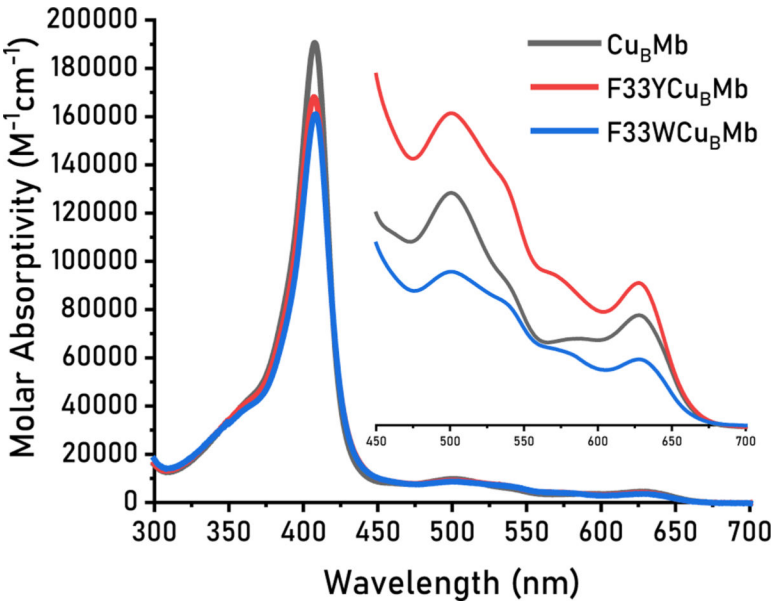

Figure 3.

UV-Vis absorption spectra of the resting state ferric forms of CuBMb (black), F33YCuBMb (red) and F33WCuBMb (blue). Inset: Expanded view of the Q band region.

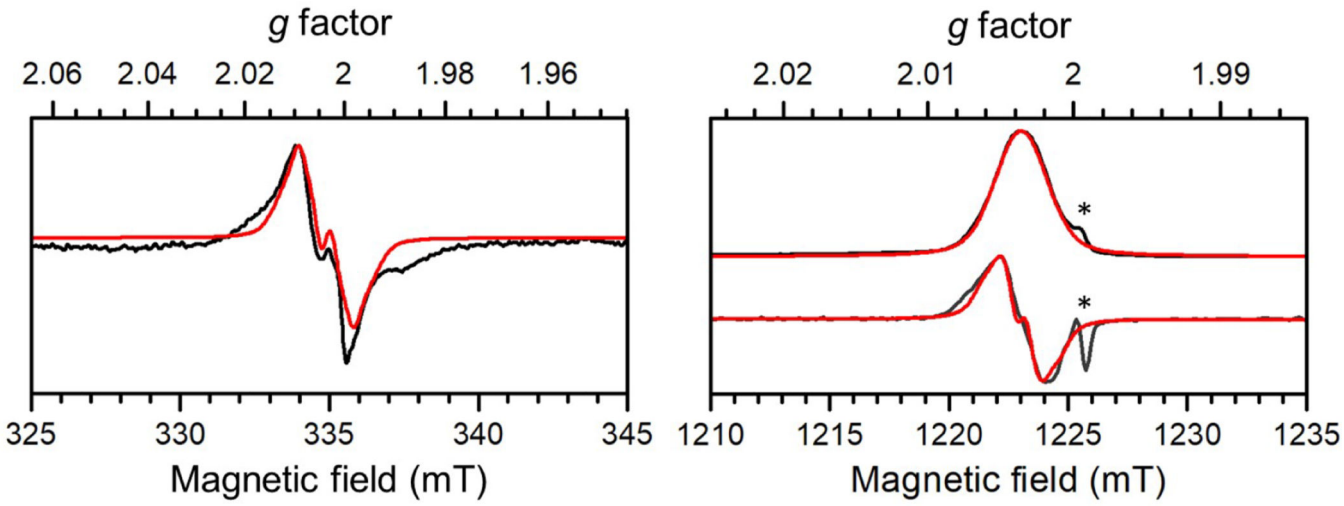

Figure 4.

X-band continuous-wave (top) and Q-band echo-detected field-sweep (bottom) EPR spectra of 5 mM F33W-Cu_BMb with 20% glycerol in 100 mM potassium phosphate buffer pH 7 after addition of 1 equiv of H_2O_2, followed by quenching at 5 s via injection into liquid N_2. Black and red lines represent data and simulations, respectively. The grey trace in the Q-band spectrum is the derivative-like plot obtained by pseudo-modulating the data at 0.2 mT. The signal denoted with an asterisk is from an impurity in the sample (g = 1.999) generated by further decomposition of the product. Experimental conditions (X-band): microwave frequency, 9.391 GHz; microwave power, 0.1 mW; temperature, 100 K; modulation frequency, 100 kHz; modulation amplitude, 3 G. Experimental conditions (Q-band): microwave frequency, 34.297 GHz; temperature, 50 K; tau, 300 ns; π/2 pulse duration, 12 ns. Simulation parameters are described in the text.